Green Synthesis of Silver Nanoparticles Using Leaf Extract of *Calluna vulgaris*: Characterizations, Properties, and Photocatalytic Activities

Gulen Oytun Akalin *

Green synthesis of silver nanoparticles was carried out using leaf extract from *Calluna vulgaris.* The formation of nanoparticles was confirmed through the emergence of a surface plasmon resonance band in ultraviolet-visible spectroscopy. The characterization conducted using various microscopic techniques revealed that the nanoparticles mostly ranged in size from approximately 20 to 70 nm. Analysis, including Fourier transform infrared spectrometry, X-ray diffraction, and energy-dispersive X-ray spectroscopy, confirmed the chemical, crystalline structure, and presence of silver, respectively. The synthesized nanoparticles exhibited notable stability with an average zeta potential of -23.1 ± 0.6 mV. Evaluation of their antibacterial activity against *Staphylococcus aureus* and *Escherichia coli* demonstrated significant efficacy with diameters of inhibition zones measuring 10.23 ± 0.54 mm and 15.38 ± 0.32 mm, respectively. Additionally, the nanoparticles displayed a remarkable inhibition of approximately 88% against *E. coli* biofilm formation at a concentration of 100 µg/mL. They also exhibited unique photocatalytic performances. This research contributes to the literature in this field by producing new silver nanoparticles with cost-effectiveness, stability, antibacterial, antioxidant, antibiofilm, and photocatalytic properties, while using a previously untapped plant extract for this purpose.

DOI: 10.15376/biores.19.3.4396-4422

Keywords: Green synthesis; Silver nanoparticles; Characterization; Antibacterial; Antibiofilm; Photocatalytic

Contact information: Medical Laboratory Program, Department of Medical Services and Techniques, Vocational School of Health Service, Aksaray University, 68100, Aksaray, Turkey;
** Corresponding author: gulenoytunakalin@hotmail.com*

INTRODUCTION

The significance of nanomaterials has grown exponentially in recent times compared to their bulk counterparts, primarily because of their unique volume ratio, extensive surface area, and various physiochemical/chemical properties (Srikar *et al.* 2016). The continuous advancements in nanotechnology have facilitated the easy production and versatile application of nanoparticles across diverse fields. Nanoparticles, characterized by dimensions within the nanoscale range (1.0 nm to 100 nm), can be derived from a variety of sources, including metals, metal oxides, polymers, dendrimers *etc*. These particles exhibit distinct types based on their size, chemical composition, physical attributes, and morphology, encompassing metal, polymeric, ceramic, semiconductor, carbon-based, and lipid-based nanoparticles (Bommakanti *et al.* 2022). While numerous chemical, physical, biological, and hybrid methods are employed for nanoparticle synthesis, it is acknowledged that chemical and physical approaches often lack eco-

friendliness and may lead to toxic effects (Srikar *et al.* 2016). Chemical methods, in particular, face challenges in terms of medical acceptance due to potential contaminations from precursor chemicals. In response to the escalating demand for environmentally friendly nanoparticles, researchers have embraced green synthesis methods to produce eco-friendly metal nanoparticles. Green synthesis offers various advantages, including energy efficiency, cost-effectiveness, and compatibility with diverse reduction methods such as photochemical reduction (Mallick *et al.* 2004), heat evaporation, electrochemical reduction, and chemical reduction. Plant extracts, rich in phytochemical compounds, such as polyols, polyphenols, flavonoids, and terpenoids, play a pivotal role in the green synthesis process (Marslin *et al.* 2018). These compounds are responsible for the bioreduction of metallic ions and act as capping agents. The functional groups within these phytochemicals actively participate in the reductive processes involved in nanoparticle formation. The adoption of 'green' and eco-friendly practices in chemistry and chemical technologies is gaining popularity globally, primarily driven by increasing environmental concerns.

Silver nanoparticles (Ag-NPs) are one of the significant widely produced nanomaterials. They have been always of interest to researchers because of their chemical stability, catalytic activity, and excellent antibacterial, anti-biofilm and anticancer properties (Du *et al.* 2016). Ag-NPs are generated through various methods, including photochemical method (Alarcon *et al*. 2012), thermal decomposition (Goudarzi *et al.* 2016), gamma ray irradiation (Chen *et al*. 2007), microwave (Khan *et al.* 2011), biological reduction (Gudikandula and Charya Maringanti 2016), electrochemical method (Reicha *et al.* 2012), laser irradiation (Abid *et al.* 2002), and hydrothermal synthesis method (Yang and Pan 2012). These methods are effective, but some methods have limitations with respect to the use of toxic and harmful reducing agents, such as citrate, $NaBH_4$ or ascorbate, high cost, and energy requirements. The interaction of these chemicals with bacterial cells can induce oxidative stress, causing severe damage to the cells.

The biological activity of nanoparticles is often linked to the bioavailability of silver ions, which is influenced by the presence of reducing agents. In this context, "green" methods for synthesizing Ag-NPs have gained prominence, specifically those utilizing biological reduction processes. These methods avoid the use of harmful chemicals, contributing to a more sustainable and environmentally friendly approach. Various plant parts, including leaves and roots are commonly employed in the green synthesis of nanoparticles due to the rich phytochemicals they contain (Marslin *et al.* 2018). The part of the plant used can be washed and boiled with distilled water for nanoparticle synthesis. When nanoparticle formation takes place, the color of the solution starts to change. The utilization of green synthesis methods, particularly biological reduction, addresses the drawbacks associated with traditional nanoparticle synthesis techniques (Gudikandula and Charya Maringanti 2016). These methods are gaining significance due to their environmental friendliness, cost-effectiveness, ease of application, and simplicity. It can be said that the use of plants as a source in the synthesis of nanoparticles is now widely preferred over other sources (microorganisms, fungi, etc.). Nanoparticles can be generated at low concentration of plant extract without using any hazardous chemicals. Ag-NPs can be prepared from many plants extracts such as mangosteen leaf (Veerasamy *et al.* 2011), *Rosa rugosa* (Dubey *et al.* 2010), *Stevia rebaudiana* (Yilmaz *et al.* 2011), *Macrotyloma uniflorum* (Vidhu *et al*. 2011), *Chenopodium album* (Dwivedi and Gopal 2010), *Ficus benghalensis* (Saxena *et al.* 2012), *Acalypha indica* (Krishnaraj *et al*. 2010), *Cycas* leaf (Jha and Prasad 2010), *Trianthema decandra* (Geethalakshmi and Sarada 2010), *Piper*

longum (Jacob *et al.* 2012), *Catharanthus roseus* (Mukunthan *et al.* 2011), *Capsicum annuum* (Li *et al.* 2007), *Nicotiana tobaccum* (Prasad *et al.* 2011), *etc*. In the literature, studies regarding the green synthesis of Ag-NPs from Ericaceae species are very rare. The extract of *Erica carnea* was chosen for the biological synthesis of Ag-NPs, and their antibacterial tests were conducted by Asiabar *et al.* (2019). The Ericaceae family comprises approximately 100 genus and 3000 species (Koroglu *et al.* 2019). *Calluna* is also a genus of plants in the Ericaceae family. The primary constituents of Ericaceae species include phenolic acids, flavonoids, tannins, and triterpenoids (Kıvçak *et al.* 2013). The leaves and flowers of Ericaceae are commonly referred to as 'puren' and 'broom bush' in Turkey. These species are extensively utilized in Turkish traditional medicine for their effectiveness as urinary antiseptic, diuretic, and against constipation (Kıvçak *et al.* 2013). In the scientific literature, extensive research has been conducted on the biological activities of *Erica* species, including anti-inflammatory (Akkol *et al.* 2008), antiulcer (Reyes Ruiz *et al.* 1996), antimicrobial (Kıvçak *et al.* 2013), and antioxidant (Pavlović *et al.* 2009; Kıvçak *et al.* 2013) properties. No study using the *Calluna vulgaris* species to produce Ag-NPs was found in the literature.

In this study, the aqueous plant extract obtained from *Calluna vulgaris* was utilized as a potential bioresource for green synthesis of Ag-NPs. This plant extract exhibited a significant role in the bioconversion of silver ions to Ag-NPs. The main aim was to devise a straightforward, economical, and environmentally friendly method for synthesizing Ag-NPs. The synthesized nanoparticles underwent a comprehensive characterization using various analytical techniques. UV-visible (UV-vis) spectroscopy, Fourier transform infrared spectroscopy (FTIR), X-ray diffraction (XRD), transmission electron microscopy (TEM), scanning electron microscopy (SEM), atomic force microscopy (AFM), energy-dispersive X-ray (EDX) and dynamic light scattering (DLS) were employed to analyse the characteristics of the nanoparticles. The stability of the nanoparticles was assessed through zeta potential measurements. Furthermore, the antioxidant, antibacterial, antibiofilm activities and photocatalytic degradation of the synthesized Ag-NPs were investigated and evaluated. This multidimensional analysis aims to provide a holistic understanding of the properties and potential applications of nanoparticles, thereby offering valuable insights to the fields of nanotechnology and bio-nanomaterials.

EXPERIMENTAL

Materials

Silver nitrate ($AgNO_3$, 99% pure), 2,2-diphenyl-1-picrylhydrazyl (DPPH), crystal violet (Sigma-Aldrich C3886) and methylene blue (MB) were obtained from Sigma-Aldrich. Antibiotic discs, Mueller-Hinton agar, tryptone soy broth, Cefoxitin FOX (30 µg) were obtained from Hitit University. Sodium borohydride, ethanol, and ascorbic acid were obtained from Merck. *Calluna vulgaris* was purchased from local herbal markets in Turkey, and it was used to obtain aqueous plant extracts. The plant material was thoroughly ground into a fine powder using a milling machine, and the powder was stored in airtight plastic containers at room temperature for extraction. All the aqueous solutions were obtained using Milli-Q water during the synthesis. The microbial strains *Staphylococcus aureus* (ATTC 25923) and *Escherichia coli* (ATCC 25922) were obtained from Hitit University Scientific Technical Application and Research Center, Turkey, where bacterial tests were also performed.

Preparation of *Calluna vulgaris* Plant Extract

Calluna vulgaris plant extract was obtained through an extraction process involving the boiling and dissolution of plant leaf parts. Distilled water served as the solvent. Approximately 2.5 g of dried plant samples were immersed in 50 mL of Milli-Q water and boiled at 80 °C for 60 min. The resulting decoctions were filtered through Whatman filter paper No. 1 (Ahmed *et al.* 2016; Erci *et al.* 2018). Following this, the aqueous solution was cooled to 4 °C over a two-day period to preserve its freshness. Subsequent to the preparation of the fresh Calluna vulgaris leaf extract, the extract was utilized in the bioreduction of Ag^+ ions for the synthesis of Ag-NPs.

Synthesis of Ag-NPs

About 5 mL of the plant leaf extract was mixed with 100 mL $AgNO_3$ solution. Ag-NPs were produced at varying $AgNO_3$ concentrations, ranging from 1.0 to 4.0 mM. Then, the mixture was stirred for 24 h at 25 °C under dark conditions to minimize photo-activation of silver nitrate (Ahmed *et al.* 2016). Following this incubation period, the bioreduction process was confirmed by observing a color change in the solution. Furthermore, the synthesis of nanoparticles was validated through UV-Vis spectroscopy. To ensure purification, the solutions underwent centrifugation at 5000 rpm for 15 min, repeated three times, with each cycle followed by washing the solution with distilled water. The resulting nanoparticles were then subjected to a vacuum medium for freeze-drying and they were preserved at 4 °C for later use. Then, they were characterized using FTIR, TEM, SEM/EDX, zeta-potential, XRD, and DLS. In addition, their antibacterial, antibiofilm, and antioxidant assays were evaluated.

Characterization of Ag-NPs

The zeta potential of Ag-NPs was assessed to understand the surface charges of these nanoparticles. Additionally, the particle size was determined using a Zetasizer, specifically the Malvern Nano ZS instrument. This analysis provides insights into both the electrostatic properties (zeta potential) and the size distribution of the nanoparticles. The information from these measurements contributes to a comprehensive characterization of the synthesized Ag-NPs, aiding in the evaluation of their stability and potential applications. UV–Vis spectroscopy is a commonly used and straightforward technique to confirm the production of nanoparticles. The spectra were recorded using an UV-Vis spectrometer (Shimadzu-UV 1800 model). The measurements were conducted in the wavelength range of min 350 nm to max 700 nm. One milliliter of the sample was added into a test tube and subsequently measured at 25 °C. The distilled water was used as a reference. The bioreduction of the Ag^+ ions ($AgNO_3$) in solution were checked by UV-Vis method. The FTIR spectrums of plant extract and green synthesized nanoparticles were taken to detect functional groups that enable the reduction of silver metal ions to nanoparticles. The FTIR analysis was made using FTIR Shimadzu IR-Prestige instrument. The samples were blended with KBr to prepare an appropriate round disc before the analysis. The analysis was performed in a wavelength range of 500 to 4000 cm^{-1}. The crystalline structure property and crystalline size were determined by XRD analysis (Diffractometer Bruker D8 Advance). The instrument was operated at Cu-Kα radiation source (λ = 1.54060 Å), with a current of 30 mA at a 2θ and voltage of 40 kV. The scanning was applied in the 2θ region of zero to 80°. The FE-SEM technique was applied for determining the morphology and size analyses of Ag-NPs. About 8 µL of nanoparticle suspensions was dropped into 200 mesh grids with a carbon support film. It was dried in

air and then fixed on a suitable SEM holder. The samples were then gold coated using a Denton vacuum desk V model coater. The SEM photos were obtained at an accelerating voltage of 30 kV using an FEI Quanta FEG 250 SEM. To confirm the presence of the Ag crystalline metallic element, EDX analysis of Ag-NPs was confirmed on a FEG-SEM equipped with an EDX attachment (Octane Pro Ametek Energy-dispersive X-ray). The shape, size, and dispersity were also researched by TEM analysis. The measurements were made by a Hitachi H-800, operating at 200 kV. The samples were obtained by putting a drop of fresh nanoparticles suspension on the TEM carbon-coated copper grid after sonicating the nanoparticles suspension. The grid was kept aside to evaporate the solvent at room temperature overnight (Sun *et al.* 2014). Atomic force microscopy (AFM Plus+ Model Microscope, NanoMagnetics Instruments) was used to analyze nanoparticles. Ag-NPs solution obtained by green synthesis was dropped into the silica glass plate. It was left to dry in the dark at 25 °C. The film glass plate was scanned with the AFM (Moosa *et al.* 2015). Dynamic light scattering method (DLS) was applied by a Zetasizer Nano ZS Instrument. The average size distributions of nanoparticles were detected in stock suspensions in distilled water. Each suspension was sonicated for 10 min and then taken in 1.5 mL cuvettes for DLS assays. Distilled water was chosen as a reference. Zeta potential measurements were determined by taking a 1.0 mL sample from the solution, placing it in a zeta potential cuvette with clean electrodes and measuring it on a Zetasizer (Malvern Nano ZS) device.

Antioxidant Activity

The DPPH radical scavenging assay was applied for determining antioxidant activity (Sreelekha *et al.* 2021). Ag-NPs (20 to 100 µg/mL) were introduced into the 0.1 mM DPPH solution and left to incubate for 30 min in darkness. The alteration in color was detected in the absorbance at 517 nm. Ascorbic acid was chosen as the reference standard. The diminished absorbance of the sample suggests increased free radical activity. The antioxidant activity (DPPH radical scavenging activity, %) was measured by Eq. 1,

$$Antioxidant\ activity\ (\%) = (Abs_{control} - Abs_{sample}) / Abs_{control} \times 100 \quad (1)$$

where $Abs_{control}$ is the absorption of control, Abs_{sample} is the absorption of sample

Antibacterial Activity

The antibacterial activity was evaluated by disk diffusion method against Gram-positive (*Staphylococcus aureus,* ATTC 25923) and Gram-negative (*Escherichia coli*, ATCC 25922) pathogens. Cefoxitin FOX antibiotic disc was used as a control group in both pathogens. The experiments were performed by Hitit University Scientific Technical Application and Research Center. The liquid culture was obtained from microorganism suspension by adjusting a 0.5 McFarland standard containing 1.5×10^8 colony units (CFU/mL). About 100 µL of culture were spread on Mueller-Hinton agar plates using a swab. Then, 10 µL of biosynthesized Ag-NPs were added into an empty disc. The disc was inserted into an agar plate. The incubation was done in 24 h at 37 °C (Ravichandran *et al.* 2016), then the inhibition zones (mm) formed around the well were recorded The values were compared to the standard antibiotic disc of Cefoxitin FOX.

Antibiofilm Activity

Escherichia coli (ATCC 25922) strain was utilized for the antibiofilm activity test. (Abishad *et al.* 2022; Singh *et al.* 2020). First, inoculation was made into 10 mL Mueller-

Hinton Broth and then, the incubation was done over 24 h at 37 °C. Mueller-Hinton Broth was employed as a control medium. Bacterial suspensions (200 µL) were dispensed into individual wells of a 96-well plate and incubated at 37 °C for 6 h. Following the initial incubation period, the culture medium was substituted with fresh medium containing different concentrations of Ag-NPs. Subsequently, the plates were further incubated at 37°C for 24 h. Upon completion of 24 h of biofilm growth, the plate was meticulously extracted and washed multiple times with sterile water to eliminate free bacteria without disturbing the biofilms. The biofilms were then subjected to staining with 0.1% crystal violet for 20 minutes (Singh *et al.* 2020). Excess dye was rinsed away with water. Ethanol (95% (v/v)) was introduced to eliminate the stain in each well, following which the optical density (OD) was determined at 590 nm (Singh *et al.* 2020). Using the average OD values, biofilm inhibition activity (%) was detected following Eq. 2:

$$Biofilm\ Inhibition\ (\%) = (OD_{control} - OD_{sample}) / OD_{control} \times 100 \quad (2)$$

Photocatalytic Degradation

To determine the photocatalytic activity of nanoparticles, 10 mg biosynthesized nanoparticles were mixed with 20 mL MB dye solution (10 ppm). Initially, $NaBH_4$ was introduced into the mixture, and the solution was stirred for 30 min in darkness to ensure nanoparticle equilibrium. Subsequently, it was exposed to sunlight for 4 h. Samples of 3 mL suspension were withdrawn from the medium to assess photocatalytic degradation. The suspension was then centrifuged at 4000 rpm for 5 min at different time intervals, and the supernatant was analyzed at 600-740 nm using a UV–Vis spectrophotometer. Photocatalytic degradation efficiency was calculated by utilizing Eq. 3 (Khan *et al.* 2016; Zheng *et al.* 2019):

$$Photocatalytic\ Degradation\ (\%) = (C_0 - C_t)/ C_0 \times 100 \quad (3)$$

C_0 is the initial dye concentration before the photocatalytic degradation, C_t is the dye concentration after photocatalytic degradation for certain time. Additionally, the reuse potential of Ag-NPs under optimal conditions was also investigated. The reusability of Ag-NPs was evaluated by repeatedly performing degradation experiments using the same nanoparticles in successive reaction cycles. Ag-NPs were taken from the reaction mixture after the degradation reaction was complete and then another reaction cycle was initiated using the same nanoparticles. This process was repeated for five reaction cycles to determine the extent of Ag-NPs reusability.

Statistical Analysis

All experiments were conducted a minimum of three times (n = 3), and the statistical mean was determined (± SD) using Microsoft 365 Excel Version 2403.

RESULTS AND DISCUSSION

Effect of the Plant Extract Dosage

The initial concentrations of the plant extract on Ag-NPs productivity were investigated. The stock solution was diluted from 1% to 100% (v/v). The total silver concentrations were measured to detect the generation of nanoparticles. The zeta potential and nanoparticle productivity (%) are given in Fig. 1. As shown in Fig. 1, the production efficiencies of nanoparticles were nearly 99.5%, 99.4%, 99.3%, 97.2%, 94.8%, and 91.1% (w/w) with 1%, 5%, 10%, 25%, 50%, and 100% (v/v) extract dilute rates, respectively. The

highest productivity of nanoparticles was detected above 98% for 1%, 5%, and 10% (v/v) extracts. The zeta potentials of the nanoparticles were close to -20 mV in 1% and 5% (v/v) extract solutions. The results are consistent with the literature. Sun *et al.* (2014) found the zeta potentials of Ag-NPs obtained from tea extracts to be -20.7 and -21.3 mV at 1% and 5% (v/v) dilution, respectively, and they stated that these values indicate the stability of AgNP suspensions. Therefore, it may be said that extracts with a zeta potential close to -20 mV are stable. The lowest nanoparticle productivity (%) was obtained with 100% (v/v) plant extract, while the highest nanoparticle productivity (%) was found with 1% and 5% (v/v) extracts. Considering both zeta potential measurements and productivity results, a 5% (v/v) extract solution was chosen for subsequent analyzes. These issues will be considered further later in the article in the context of distributions of zeta potential values.

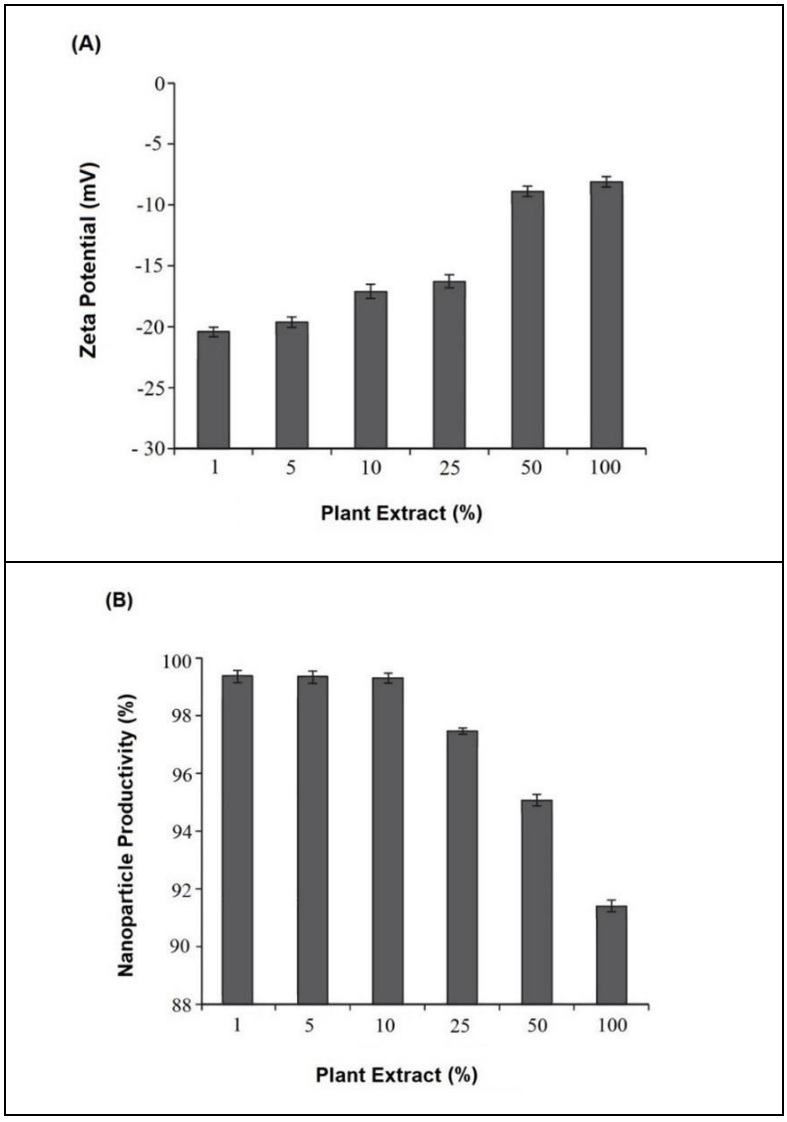

Fig. 1. Effects of plant extract (%) on (a) zeta potential; and (b) nanoparticles productivity (Each value represents the mean ± SD of three replicates)

UV-Visible Studies

UV-Vis spectroscopy was employed to monitor the synthesis and stability of nanoparticles. According to the literature, metal nanoparticles exhibit a surface plasmon resonance (SPR) absorption band because of the presence of free electrons vibrating mutually in resonance with the light wave (Anandalakshmi *et al*. 2016). Depending on their concentration and size, silver nanoparticles result in the formation of a dark color, which is attributed to their excitation of SPR of Ag-NPs. (Prakash *et al*. 2013). Fig. 2 displays the UV–Vis spectra of Ag-NPs biosynthesized from *C. vulgaris* plant extract. The characteristic SPR peak and the color changing are clearly apparent in Fig. 2(a).

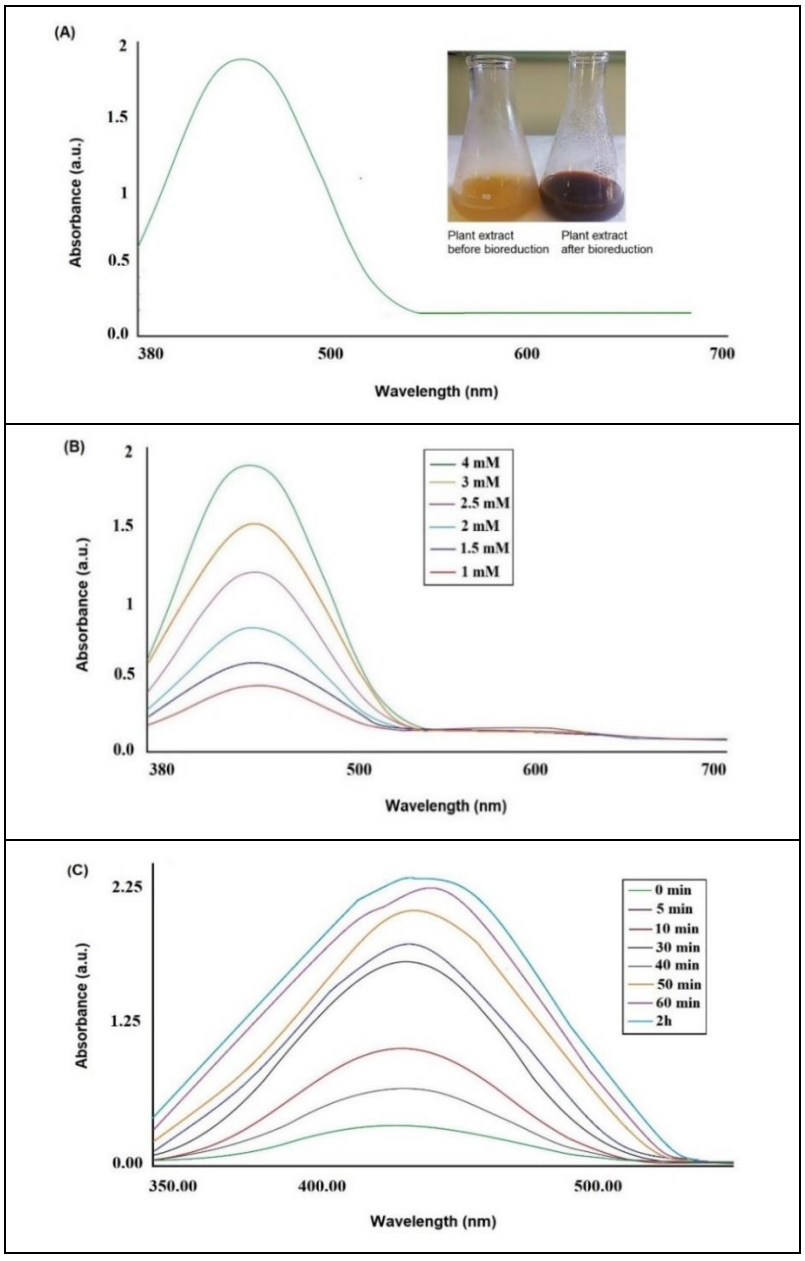

Fig. 2. (a) UV–Vis spectra of synthesized Ag-NPs from *C. vulgaris* leaf extract; (b) UV–Vis spectra of synthesized Ag-NPs from *C. vulgaris* leaf extract at different $AgNO_3$ concentrations; and (c) The effect of reaction time on Ag-NPs synthesis utilizing *C. vulgaris* leaf extract

The shift in color indicates the presence of Ag-NPs.The SPR peak was found to be at nearly 435 nm. It is well known that the maximum wavelength in range of 400 to 500 nm is specific for Ag-NPs because of their SPR excitation (Prakash *et al*. 2013; Jyoti *et al*. 2016; Li *et al*. 2020). Zaheer *et al.* (2012) reported that the SPR peak of Ag-NPs located around 425 nm is the specific extinction coefficient of small monodispersed spherical Ag-NPs. Kanniah *et al.* (2021) found that the specific SPR peak was at about 430 nm. They explained that the ketones and carboxylic acids acted as both stabilizing and reducing agents. Bar *et al.* (2009) explained that the increase in particle size causes the shifting of SPR band and bandwidth to increase.

As shown in Fig. 2(b), the absorbance was influenced directly with the concentration of $AgNO_3$. Similar result was reported by Ahmed *et al.* (2016). Absorbance changes up to 2 h are also given in Fig. 2(c). Spectra were taken at certain time intervals to measure stability. The stability of nanoparticles was found to continue for more than 2 h. The increment of the absorbance may indicate the formation of more synthesized nanoparticles. According to the findings, Ag-NPs synthesized by *C. vulgaris* leaf extract can be considered stable. Using the UV–Vis spectrum, it was verified that $AgNO_3$ was reduced to nanoparticles due to the presence of the *C. vulgaris* plant extract.

FTIR Analysis Results

The chemical composition of Ag-NPs was examined by FT-IR spectroscopy. The spectra of Ag-NPs extracted from *C. vulgaris* leaf (after bioreduction) and control sample of dried *C. vulgaris* leaf extract (before bioreduction) are given in Fig. 3. Mostly similar peaks were observed in both spectra. The broad band 3000-4000 cm^{-1} may be due to the -OH groups. This band may indicate the availability of phenol and alcohol groups. Li *et al.* (2020) reported that -OH stretching vibration may be due to resulting from polyphenols or polysaccharides in the extract and −OH groups are vital for the green synthesis of Ag-NPs. Two small peaks observed at ~3280 and ~3200 cm^{-1} may indicate the presence of primary amines (N–H stretching). The bands at ~2923 and ~2858 cm−1 region may signify the H-C-H symmetric and asymmetric stretching (Li *et al.* 2020). The band at ~1750 cm^{-1} may have risen from C=O stretching of ketones, aldehydes, and carboxylic acids. Kanniah *et al*. (2021) explained that the ketone is a reducing agent that effects the reduction of metal ions to metal nanoparticles. Similarly, Ulug *et al.* (2015) clarified that some or combination of C=O, N-H, C-H, O-H, C-O, C-N, and C≡C bands may reduce silver ions to form Ag-NPs. The band at ~1600 cm^{-1} in the plant extract spectra may be due to amide 1 vibrations. The similiar band has slightly shifted to around ~1611 cm^{-1} in the nanoparticle spectra. The result is consistent with the literature. Prakash *et al.* (2013) observed similar difference for plant and nanoparticles. They explained that the peak at ~ 1618 cm^{-1} observed in plant leaf corresponds to amide I vibrations, and in Ag-NPs, this peak shifted to ~1623 cm^{-1}, probably due to the binding between amine groups and Ag-NPs. The bands ~1375 cm^{-1} may be accurred from O–H/N–H bending vibrations. Somasundaram *et al.* (2021) stated that O–H/N–H bending vibrations were observed at ~1325 cm^{-1} in green synthesized Ag-NPs. They also explained that during nanoparticle production, the presence of carboxylate and hydroxyl groups increases the binding of Ag^+ ions, thus reducing silver ions to elemental silver. In other words, they said that carboxylate and hydroxyl groups play an important role in obtaining silver nanoparticles. Additionally, the band observed at approximately ~1040 cm^{-1} is thought to be related to C-O-C stretching (Prakash *et al.* 2013).

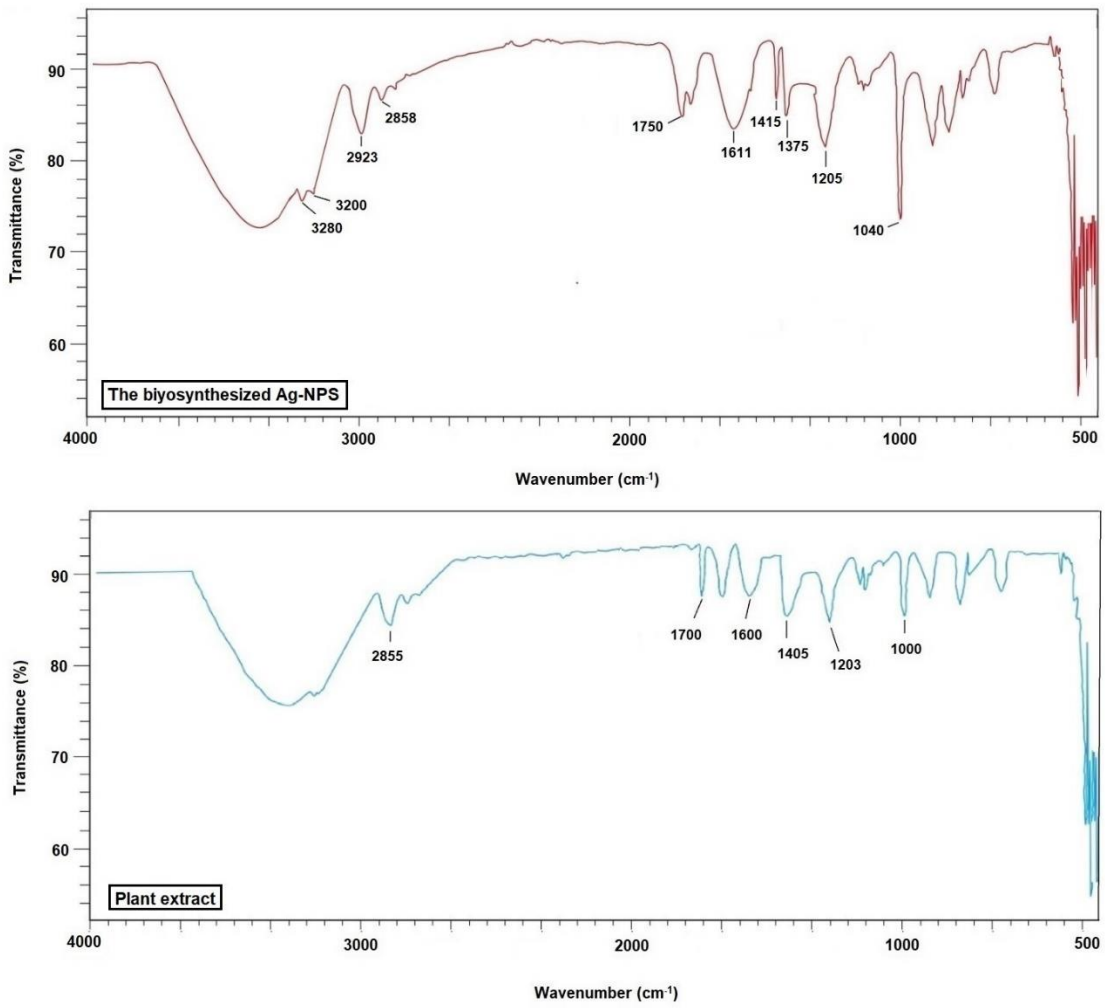

Fig. 3. FTIR spectra of the biyosynthesized Ag-NPs; and the plant extract

XRD Results

The crystalline structure of biosynthesized nanoparticles was examined by XRD. The measurement depends on the diffraction patterns. Materials can be identified by comparison with JCPDS reference (Joint Committee on Powder Diffraction Standards) library. The JCPDS number of the standard metallic silver XRD pattern is 04-0873 (Li *et al*. 2020; Singla *et al*. 2022). The XRD can also indicate the purity of the materials. The study of X-ray diffraction is based on Bragg's law (Zhang *et al.* 2016). The definition of Bragg reflections relates the (111), (200), (220), and (311) sets (Li *et al*. 2020). The XRD pattern of the synthesized nanoparticles is displayed in Fig. 4. The XRD pattern showed that four Bragg reflections were observed at 38.95°, 44.78°, 64.88°, and 77.75°, which were related to (111), (200), (220), and (311) crystal planes. The results are in good agreement with literature. Jyoti *et al.* (2016) found four strong Bragg reflections at 38.45°, 46.35°, 64.75°, and 78.05° corresponds to the planes of (111), (200), (220), and (311), respectively. Li *et al.* (2020) indicated that the diffraction peaks of metallic silver were observed at 2θ values of 38.16° (111), 44.40° (200), 64.58° (220), and 77.38° (311). They stated that the high intensity diffraction peak found at 2θ of 38.16° corresponding to the

crystalline silver. Four diffraction peaks in the 2θ region of 38.12° (111), 44.31° (200), 64.43° (220), and 77.39° (311) was found by Singla *et al.* (2022). Khalil *et al*. (2014) found that four diffraction peaks at 2θ of 38.17°, 44.31°, 64.44°, 77.34°, and 81.33° could be attributed to crystallographic planes. The average size of nanoparticles was calculated with Debye–Scherrer equation (Eq. 4),

$$D = k\lambda/\beta\cos\theta \quad (4)$$

where k is a geometric factor to 0.9, D is average diameter size, λ is the wavelength of X-ray radiation source (1.54060 Å), θ is the diffraction angle, and β is the full width at half maximum (FWHM) (Kanniah *et al.* (2021). The average diameter size was measured at 44.77 ± 0.5 nm. It can be said that the result is in accordance with literature. Kanniah *et al.* (2021) and Khalil *et al.* (2014) found the average size of Ag-NPs using with Debye–Scherrer equation to be ~ 34.79 nm and ~ 51nm, respectively.

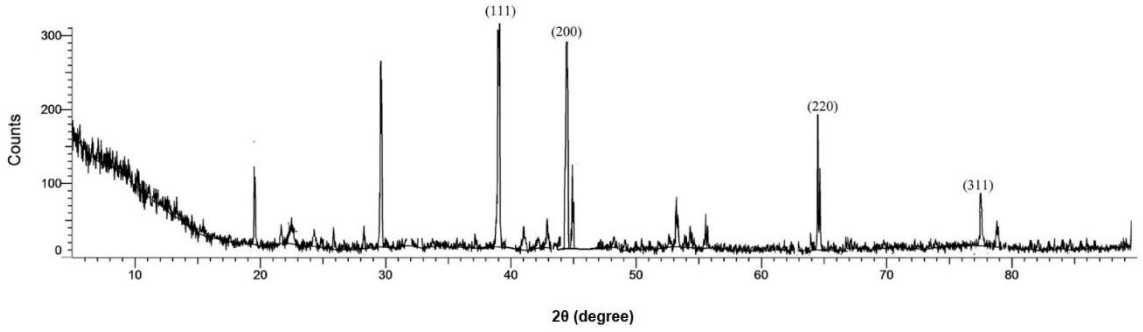

Fig. 4. XRD pattern of biosynthesized Ag-NPs

SEM/EDX, TEM, and AFM Analyses

TEM and SEM images of biosynthesized Ag-NPs are presented in Figs. 5 and 6. The particle size of the nanoparticles was detected to be below 50 nm in TEM analysis. Particles with sizes of 20 or 30 nm, mostly spherical in shape, are clearly visible in the TEM images (Fig. 5b and 5c). The SEM analysis clearly indicated the presence of nano-sized particles (40 to 70 nm) in Fig. 6(a) and 6(b). The nanoparticles, mostly spherical but occasionally hexagonal, could be seen in SEM images. The results are consistent with the literature. Li *et al*. (2020) prepared Ag-NPs from corn silk aqueous extract. They found that the particle sizes were from 10 nm to 30 nm in SEM images. Elumalai *et al.* (2017) observed that nanoparticles synthesized from leaf extracts of *Hyptis suaveolens* and *Leucas aspera* were predominantly spherical and quasispherical in SEM images. Additionally, they observed that the formation of Ag-NPs with various shapes included spherical, triangular, hexagonal and polyhedral particles in TEM images. The AFM image and the particle size distribution of nanoparticles is given in Fig. 7. The average diameter size was found to be approximately 49.8 nm. This finding agrees with SEM and TEM images. Therefore, the synthesized Ag-NPs were shown to be nano-sized by SEM, TEM, and AFM analyses. Additionally, the presence of silver was demonstrated by the EDX spectrum. As seen from Fig. 6(c), the strong absorbance peak in the silver region at 3 keV verified the synthesis of Ag-NPs (Guzman *et al.* 2012; Kanniah *et al*. 2021). The weight (Wt%) and atomic (At%) fraction values obtained by EDX analysis are given in Fig. 6(c). The Wt% values of silver (56.27%) were higher than those of carbon (10.64%) and oxygen (33.09%). A similar difference was observed for At% values. Jyoti *et al*. (2016) stated that in addition

to a strong signal of silver, there is also a weak oxygen peak in EDX spectrum and that this peak may be due to biomolecules bound to the surface of Ag-NPs. This could indicate that silver ions had been reduced to elemental silver Jyoti *et al*. (2016). The findings may further suggest the high purity of the synthesized nanoparticles.

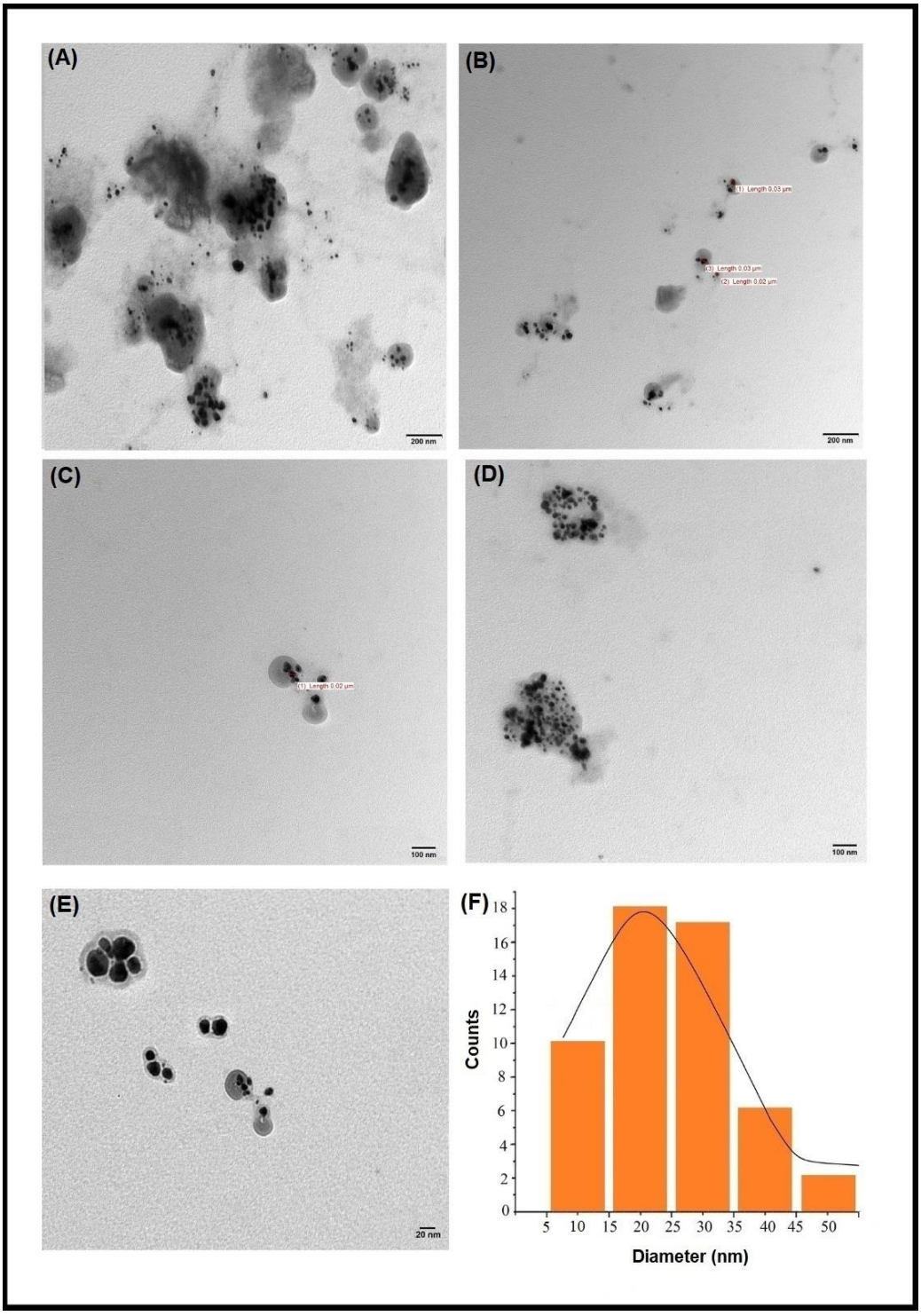

Fig. 5. TEM images and the particle diameters of Ag-NPs

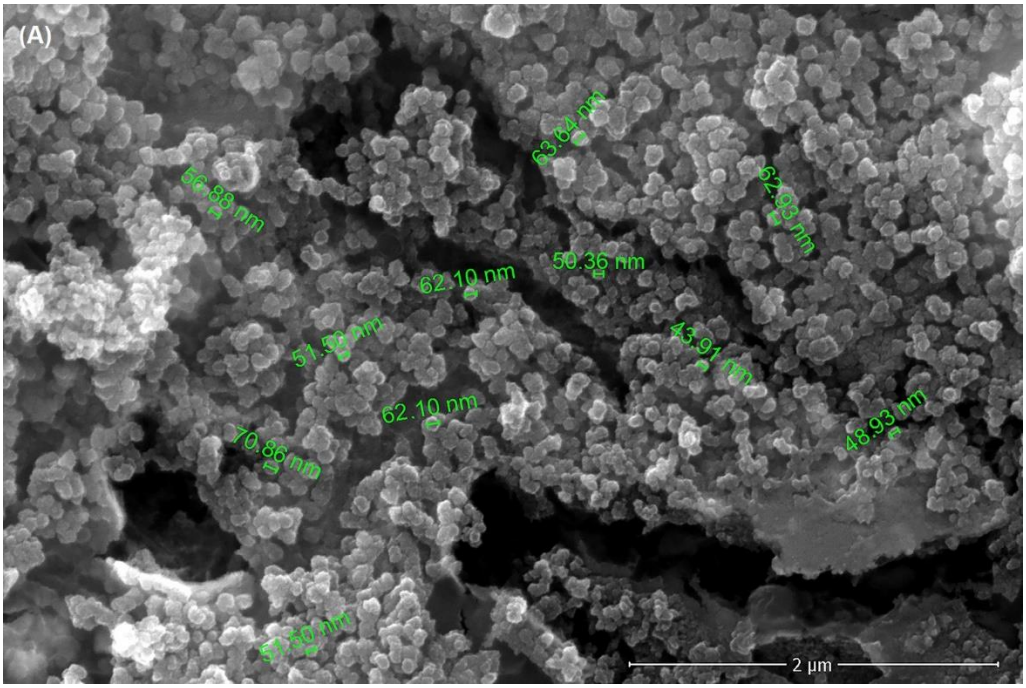
(A)
63.64 nm
62.93 nm
50.36 nm
62.10 nm
51.50 nm
43.91 nm
62.10 nm
70.86 nm
48.93 nm
51.50 nm
2 µm

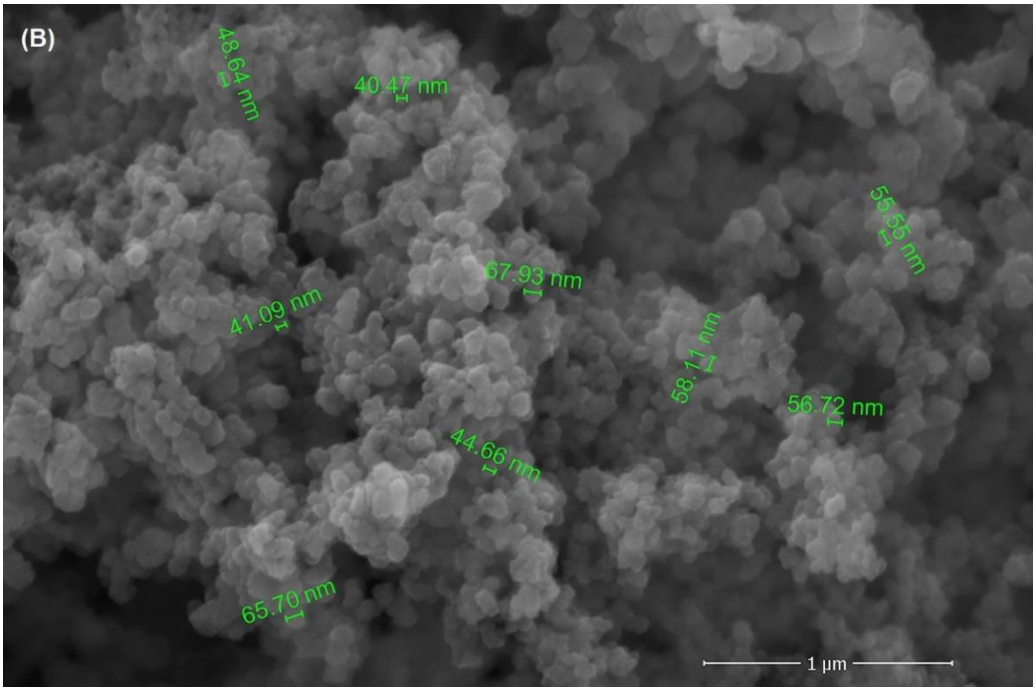
(B)
48.64 nm
40.47 nm
55.55 nm
67.93 nm
41.09 nm
58.11 nm
56.72 nm
44.66 nm
65.70 nm
1 µm

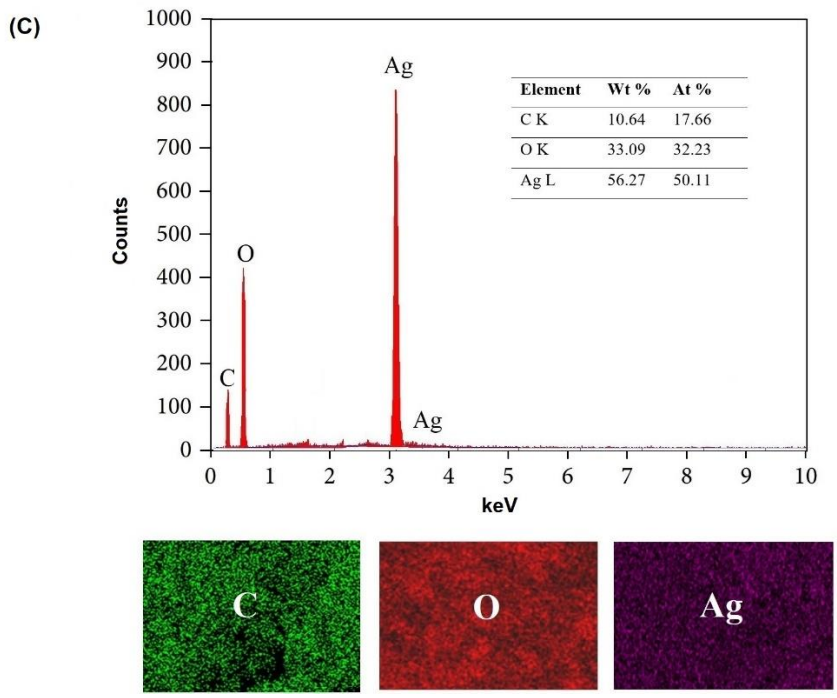

Fig. 6. SEM images of Ag-NPs at magnification (a) 2 µm; (b) 1 µm; and (c) EDX spectrum of Ag-NPs

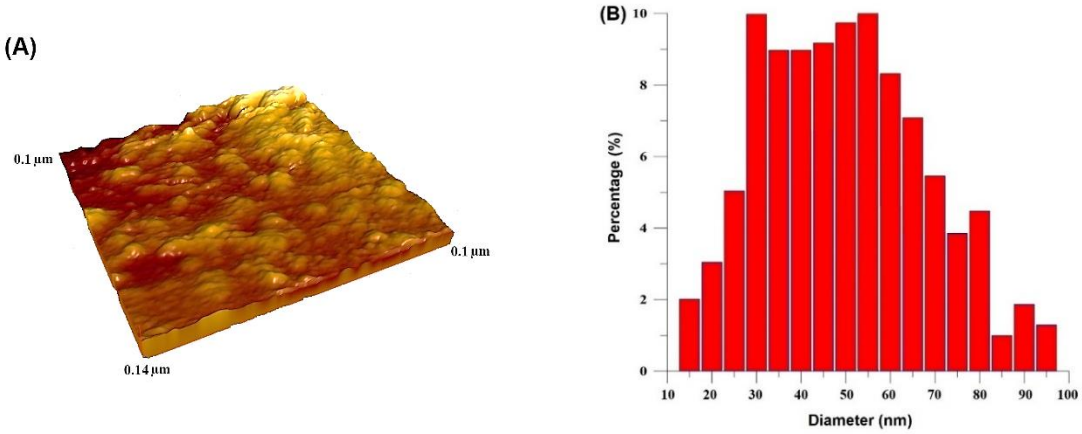

Fig. 7. (a) AFM images; and (b) the particle size diameters of nanoparticles

Zeta Potential and DLS of Ag-NPs

The particle size and distributions were measured by DLS to characterize the physical stability of the nanoparticles. Size distribution and zeta potential provide valuable information about the stability, homogeneity, and sizes of the synthesized nanoparticles. The particle size distribution of the nanoparticles is given in Fig. 8(a). The particles sizes were ranged from 10 to 80 nm. According to the results, the particle sizes measured from DLS are detected slightly larger than those from TEM. The findings are in line with the literature. Zhang *et al*. (2016) explained that the particle sizes differences between DLS and TEM results might have occurred due to the effectiveness of Brownian motion.

Another reason for particle size differences between DLS and TEM results may be the preparation conditions. The sample is dried under vacuum in TEM, whereas the samples are dispersed in a liquid medium in DLS (Zhang *et al*. 2016). The TEM is a technique related to the number of nanoparticles, while DLS is related to the density (Flores-Ramírez *et al*. 2023). DLS disperses particles within a solution, facilitating their solvation, whereas TEM operates on desiccated samples under conditions of ultrahigh vacuum. The DLS technique measures the hydrodynamic radius of dispersed particles, whereas TEM displays surface area thanks to the incident electrons that pass through the sample (Flores-Ramírez *et al*. 2023). Consequently, the size obtained by DLS is generally larger compared to TEM.

Zeta potential results are given in Fig. 8(b). Clogston and Patri (2011) indicated that nanoparticles with a zeta potential between -10 and +10 mV are considered nearly neutral, while those with zeta potentials exceeding +30 mV or dropping below -30 mV are characterized as strongly positively charged and strongly negatively charged, respectively. It can be said that the biosynthesized Ag-NPs are considered mostly negatively charged in Fig. 8(b). There may be some electrostatic attractions between the particles except in the part where the distribution of zeta potentials is neutral. These attractions can affect the distribution of charges on the surfaces of nanoparticles. These interactions can lead to rapid between some of the particles, potentially affecting the stability of nanoparticles.

The stability may be affected with components such as hemicellulose found in plant material. These components can provide steric stabilization by adsorbing on the surfaces of nanoparticles. Steric effects resulting from the adsorption of molecules to the surface can prevent electrostatic attractions between particles, so these components may lead to the particles becoming more stable. There are supporting references regarding this situation in the literature. Kwon *et al.* (2020) examined the adsorption properties of Ag-NPs with different lignin and hemicellulose contents. Significant binding interactions were observed between surface functional groups between Ag-NPs and cellulose nanofibrils. Therefore, it can be said that the cellulose composition significantly affects the adsorption of Ag-NPs. Naidjonoka *et al.* (2021) explained that hemicellulose provides steric stabilization mechanism through chains with high molecular weight. They also suggested that hemicellulose may partially affect the zeta potential of nanoparticles. This further strengthens the positive effect of hemicellulose on the stability of nanoparticles. These studies strengthen the proposed idea that hemicellulose may play a role in the stabilization of nanoparticles.

At the maximum total counts value, the zeta potential value was nearly -23.1 ± 0.6 mV in Fig. 8(b). The result is in accordance with the literature. The zeta potential of synthesized Ag-NPs from *Asphodelus aestivus Brot. aerial* part extract was measured as −22.2 mV by Fafal *et al*. (2017). Patil *et al.* (2012) found that the average particle size and zeta potential of Ag-NPs synthesized by latex from *J. gossypifolia* were 62.09 nm and −29.7 mV, respectively. It was explained that the negative zeta potential value increased the stability of the nanoparticles and prevented agglomeration (Patil *et al.* 2012, 2018). Similarly, Mukherjee *et al*. (2014) identified the nanoparticles with zeta potential between -10.1 ± 0.7 and -15.2 ± 0.5 as negatively charged. They also reported that the high negative potential value contributes to the long-term stability, high dispersity, and good colloidal property of nanoparticles because of their negative-negative repulsion. Additionally, Rao *et al.* (2013) found the zeta potential of the synthesized Ag-NPs to be -55.0 mV, and its negative value was associated with an increase in the repulsion between the particles, thus enhancing the stability of the formulation. Jyoti et al. (2016) stated that the nanoparticles with an average zeta potential value of -24.1 mV are negatively charged. In another study,

the average particle size was found to be 30.2± 2.1 nm, whereas the zeta potential value was -20.17 mV (Wang *et al.* 2018). It was suggested that the synthesized silver nanoparticles exhibited a satisfactory level of stability and dispersion (Wang *et al.* 2018).

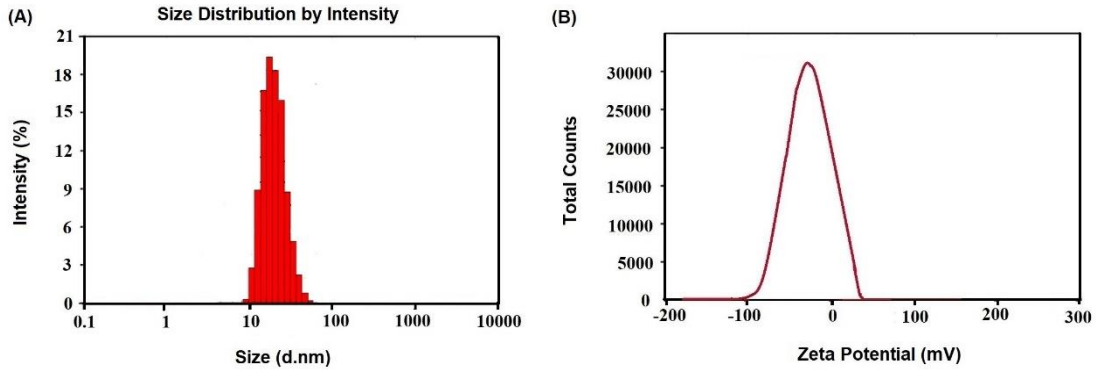

Fig. 8. (a) The particle size distribution; and b) zeta potential of nanoparticles

Antibacterial Activity, Antioxidant Activity, and Antibiofilm Studies

The antibacterial effects of biosynthesized Ag-NPs on Gram-negative bacteria (*E. coli*) and Gram-positive bacteria (*S. aureus*) were assessed using the disk diffusion assay. (Erci *et al.* 2018). Ag-NPs displayed antibacterial activity against both Gram-positive and Gram-negative bacteria. The images are shown in Figs. 9(a) and 9(b). The zone diameters (mm) are given in Fig. 9(c).

The inhibition zone of Ag-NPs against *E. coli* was 15.38 ± 0.32 mm, while an inhibition zone of 10.23 ± 0.54 mm was observed for *S. aureus.* The Gram-negative and Gram-positive bacteria exhibited different zone diameters. These findings are compatible with the literature. Erci and Torlak (2019) observed the differences in the inhibition zones of Gram-negative bacteria and Gram-positive bacteria. The lower effect of nanoparticles on Gram-positive bacteria may be related to the zeta potential. Domínguez et al. (2020) stated that the peptidoglycan layer composing the cell wall of Gram-positive bacteria bears a negative charge, and the amount of peptidoglycan is higher than Gram-negative bacteria. They also explained that the thick and dense peptidoglycan layer of Gram-positive bacteria effectively prevents silver ions from adhering to and penetrating the cell wall, thus giving the bacteria resistance to silver. In other words, cell entry and inhibition may have been difficult due to electrostatic repulsion between negatively charged Ag-NPs and negatively charged Gram-positive bacteria. Similarly, Ansari *et al.* (2021) and Arshad *et al.* (2018) found that synthesized A-NPs exhibited greater sensitive against Gram-negative bacteria compared to Gram positive bacteria. The findings, aligning with existing literature, unequivocally underscore the heightened effectiveness of Ag-NPs against Gram-negative bacteria. These comments, based on the distinctive charge properties of Ag-NPs and the chemical composition of bacterial cell walls, elucidate the underlying causes. Biosynthesized nanoparticles have demonstrated potent antibacterial properties, making them promising candidates for combating bacterial infections.

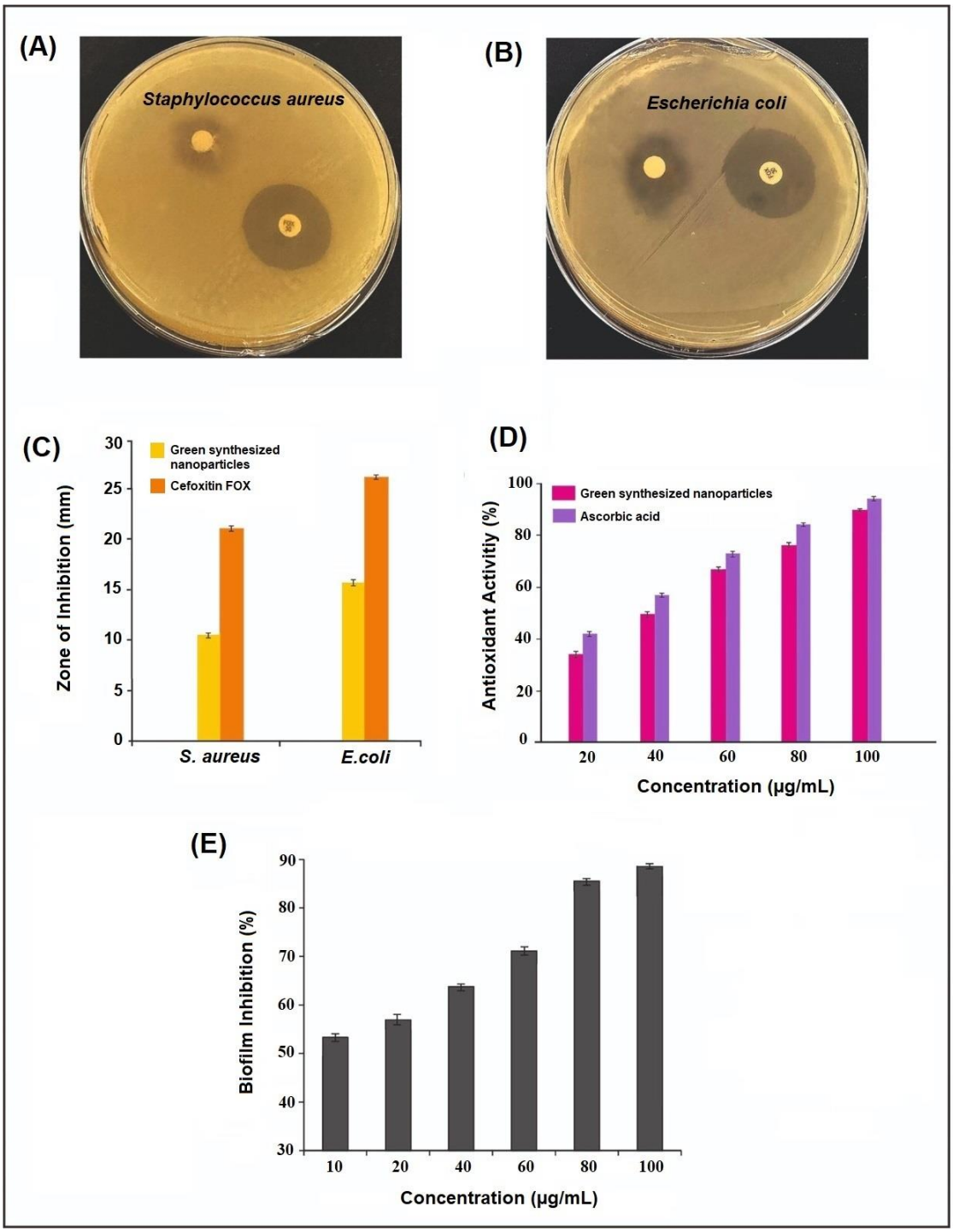

Fig. 9. (a), (b), and (c) Zone of inhibitions of Ag-NPs against *S. aureus* and *E. coli*; (d) Antioxidant activity of biosynthesized Ag-NPs; and (e) Antibiofilm activity of biosynthesized Ag-NPs. Each value represents the mean ± SD of three replicates

The DPPH assay is mostly preferred in antioxidant analysis because it is easy and rapid to use. Begum *et al.* (2022) explained that antioxidants can be used alone or in synergism in various diseases (such as diabetes, cardiovascular disease, diabetes, or cancer) by scavenging free radicals. As is known, DPPH is a stable free radical that displays the

maximum absorption at 517 nm and has a purple color (Sreelekha *et al*. 2021) In the presence of an antioxidant, the color changing takes place and the absorbance decreases because of free radical pairing in DPPH. In other words, DPPH radicals are donated electrons by Ag-NPs and the radicals are reduced. The color change from purple to yellow during the experiment is an indicator of antioxidant activity (Begum *et al.* 2022)

Fig. 9(d) displays the antioxidant activities of biosynthesized Ag-NPs. Ascorbic acid was utilized as a control. As the concentration of Ag-NPs increased from 20 to 100 μg/mL, the antioxidant activity showed a corresponding increase. The highest antioxidant activity (~89%) was observed at a concentration of 100 μg/mL.The results reveal that the green synthesized Ag-NPs exhibited good antioxidant activities. The IC_{50} value of Ag-NPs was calculated to be nearly 56.2 μg/ mL. The results are consistent with the literature. Ravichandran *et al*. (2016) found that DPPH radical scavenging activity % affected directly with Ag-NPs concentration and the maximum antioxidant activity was found to be 79.79% at 100 μg/mL. The IC_{50} value was 51.17 μg/mL. The antioxidant ability could be attributed to the functional groups adhered to them. As is known, flavonoids and phenolic compounds can display excellent antioxidant activity. (Marslin *et al.* 2018). Similar results were obtained by Wei *et al*. (2021). They found that the radical scavenging activity % of Ag-NPs derived from Chinese herbal medicines was 85.8% at 100 μg/mL. They explained that the plant extract can be used both as an antioxidant to neutralize free radicals and in the treatment of many diseases caused by oxidative stress.

Biofilm provides an important protection opportunity against external factors for organisms living within it, particularly rendering pathogens more resistant to environmental changes. Microorganisms forming biofilms behave differently from free-living organisms in terms of growth rates and resistance they develop against antimicrobial treatments, thereby posing a public health concern. One of the commonly employed methods to completely eradicate or prevent the development of biofilms is to use effective materials to remove biofilms or prevent bacterial adhesion. The use of nanomaterials for this purpose is considered one of the most promising strategies in combating biofilm infections. Nanomaterials can inhibit bacterial adhesion and biofilm formation. Fig. 9(e) illustrates the percentages of biofilm inhibition at various nanoparticle concentrations ranging from 10 to 100 μg/mL. Within this concentration range, it was observed that the biofilm inhibition (%) significantly increased with the nanoparticle concentration, indicating a notable concentration-dependent effect on biofilm inhibition. Particularly noteworthy is the highest inhibition rate recorded at nearly 88% for biofilms formed at a concentration of 100 μg/mL. The findings obtained align with existing literature. For instance, Gupta *et al.* (2014) reported that Ag-NPs obtained by *Psidium guajava* L. leaf extract demonstrated antibiofilm activity exceeding 80% against *E. coli* bacteria. Similarly, Du *et al.* (2016) demonstrated that biosynthesized Ag-NPs effectively inhibited the biofilm formation of *E. coli.* The findings collectively highlight Ag-NPs, synthesized with *C. vulgaris* leaf extract through green synthesis, possess significant antibacterial, antioxidant and antibiofilm effects across various nanoparticle concentrations. The antioxidant, antibacterial and antibiofilm properties of silver nanoparticles synthesized from *C. vulgaris* leaf were identified for the first time in this study. These findings suggest that Ag-NPs biosynthesized in this study may hold potential for use in medicine, industry, and various other application areas. Furthermore, these results underscore that Ag-NPs obtained through green synthesis methods can broaden the scope of the application areas.

Photocatalytic Degradation

Photocatalytic degradation encompasses the interaction between photons and a catalyst. Electrons associated with an isolated atom occupy specific energy levels (Khan *et al.* 2016). However, within a crystal structure, these energy levels divide into multiple levels corresponding to the atoms present. Consequently, the energy levels become closely packed, resembling a continuous band of energies (Khan *et al.* 2016). In the scenario of metals or conductors, the highest energy band is typically half-filled, enabling electrons in this band to transition into the unoccupied portion with minimal energy input. Upon interaction with metal nanoparticles, visible light photons stimulate metal electrons (conduction electrons) through the surface plasmon resonance effect, initiating the process of MB reduction (Khan *et al.* 2016). The catalytic activity of nanoparticles is predominantly dictated by their reduction potential during the catalytic process. Nanomaterials demonstrate enhanced catalytic activity owing to their negative redox potential relative to their bulk forms (Khan *et al.* 2016). As a result, Ag-NPs are highly efficient photocatalysts for reducing organic dyes under visible light.

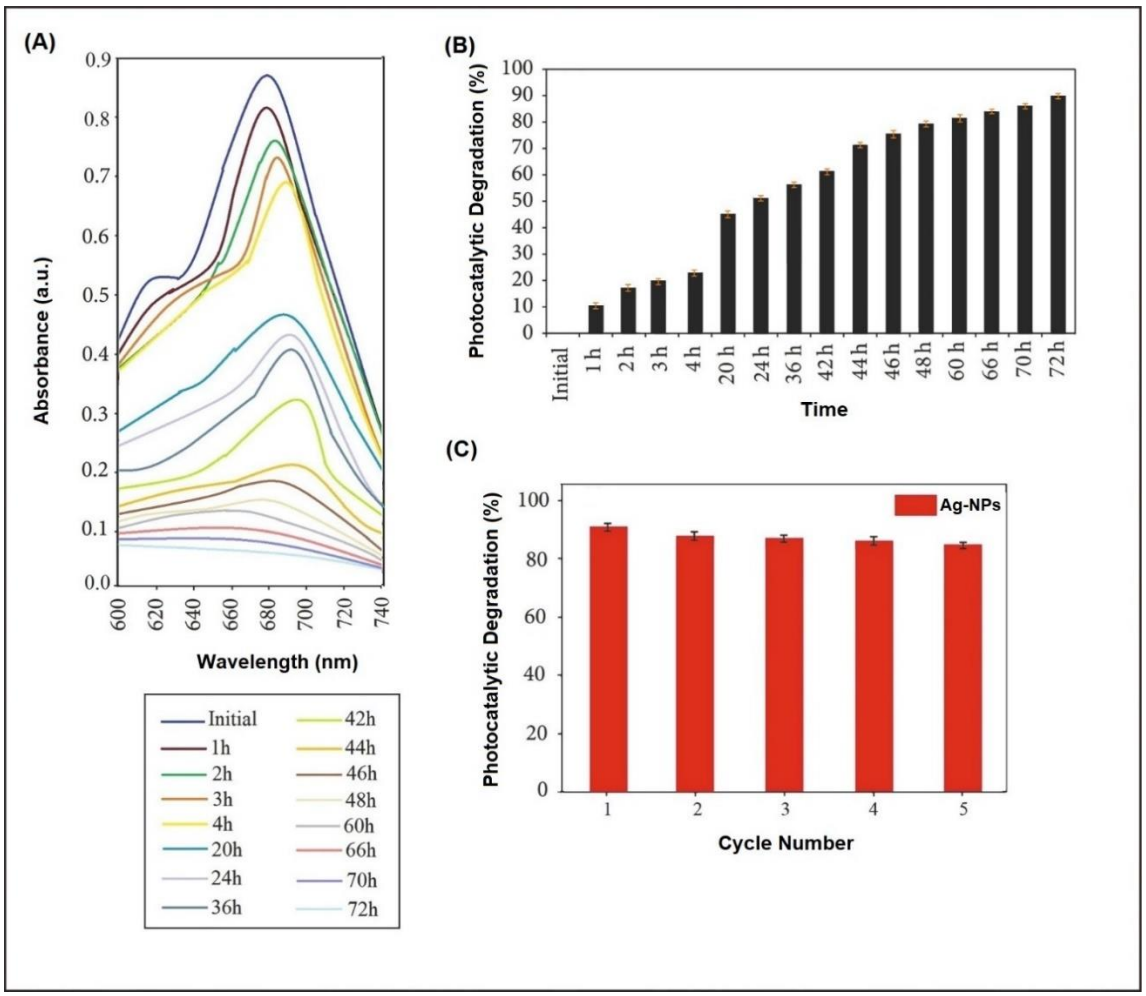

Fig. 10. (a) The absorption spectra of aqueous solution of MB treated with Ag-NPs synthesized from *C. vulgaris* leaf extract at different time intervals; (b) Percentage of photocatalytic degradation by synthesized Ag-NPs at different time intervals; and (c) Reusability of the synthesized Ag-NPs.

Figure 10(a) demonstrates the photocatalytic performance of the synthesized Ag-NPs on MB. In this examination, the duration of light exposure was assessed as a parameter. The distinctive absorption peak of MB was detected nearly 670 nm. The findings reveal that with prolonged exposure to light, there is a proportional enhancement in MB degradation, coupled with a gradual reduction in the intensity of the absorption peak. By the conclusion of 72 hours, degradation approached nearly 90% (Fig. 10b). The photocatalytic capabilities of Ag-NPs under visible light are likely triggered by the excitation of surface plasmon resonance (SPR), while oscillations in charge density may play a crucial role in interfacing between different phases and dielectric media (Miri et al. 2018). Consequently, acting as an electron donor, Ag-NPs alter the chemical characteristics of the dye, counteracting its adverse impacts. As a consequence of the electron transfer from Ag-NPs to MB, a notable outcome is the reduction in the intensity of the MB absorption peak (Khan *et al.* 2016; Miri et al. 2018).

The ability to recycle a photocatalyst is essential for cost-effective industrial applications (Kalaycıoğlu *et al.* 2023). The reusability of nanoparticles was evaluated over five repeated cycles, as depicted in Fig. 10(c). In the second cycle, dye removal decreased slightly to nearly 87%. However, by the fifth repeat cycle, the photocatalyst still exhibited over 80% removal efficiency, indicating the reusability of nanoparticles. These findings underscore the practicality and sustainability of employing such photocatalysts in industrial processes.

A potential mechanism of MB degradation in the presence of the prepared Ag-NPs is presented in Scheme 1 (Khan *et al.* 2016; Yang *et al.* 2017). The results of this study suggest that the biosynthesized Ag-NPs can be effectively utilized in the industry for the detoxification of various dyes because of their catalytic properties. According to the literature, in aqueous solution, MB is reduced to leuco-methylene blue (LMB) and MBH_2^+ to form stable and colorless compounds (Somasundaram *et al.* 2021). In other words, MB can be reduced to colorless leuco forms (degraded products) by the presence of reducing agents. (Somasundaram *et al.* 2021).

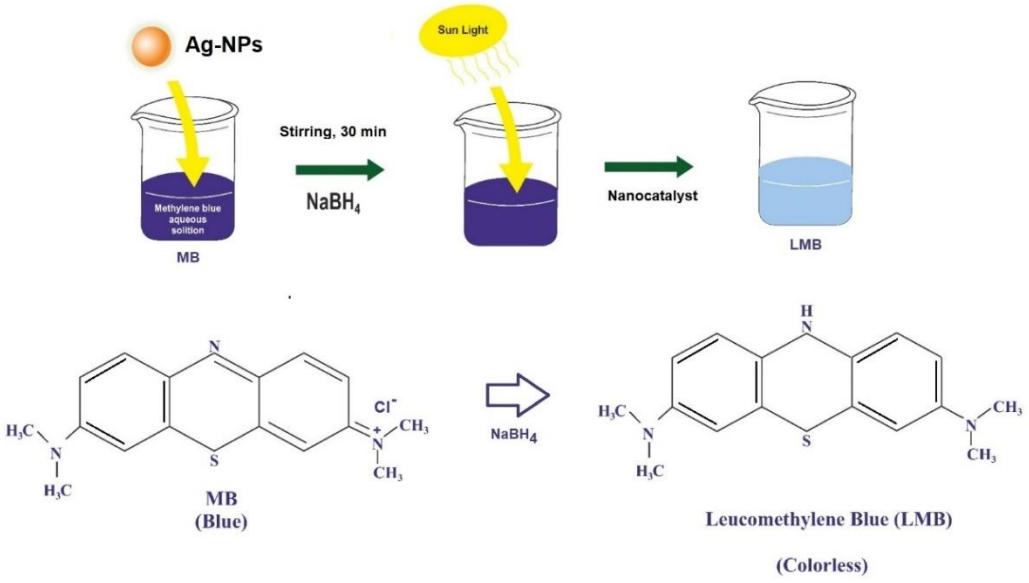

Scheme 1. A potential mechanism of MB degradation in the presence of the prepared Ag-NPs

The Langmuir–Hinshelwood model was used to elucidate the potential mechanism behind the catalytic degradation of MB by Somasundaram *et al.* (2021). They stated that $NaBH_4$ plays a dual role as both an electron donor and a hydrogen supplier, while Ag-NPs act as intermediaries in transferring electrons between the BH_4^- ion and MB due to their high negative potential. They also explained that upon the introduction of $NaBH_4$ into a solution containing MB and Ag-NPs, the BH_4^- ion from $NaBH_4$ and MB molecules adsorb onto the surface of the Ag-NPs, facilitating rapid electron and hydrogen transport. Diffusion among the adsorbed molecules can lead to the desorption of the colorless degraded by-product, potentially providing additional catalytic sites for the degradation of MB due to the extensive surface area of Ag-NPs (Panáček *et al.* 2014; Somasundaram *et al.* 2021).

CONCLUSIONS

1. A new contribution to the green synthesis literature was made by preparing Ag-NPs from *Calluna vulgaris* leaf extract. The production of silver nanoparticles is clearly evidenced from detecting the surface plasmon resonance (SPR) band in the UV-Visible spectra.
2. The nanoparticle sizes of the biosynthesized Ag-NPs were measured by scanning electron microscopy (SEM), transmission electron microscopy (TEM), atomic force microscopy (AFM), and dynamic light scattering (DLS). The average zeta potential was detected as approximately -23.1 ± 0.6 mV, and the crystalline property was analyzed using X-ray diffraction (XRD) analysis.
3. Biosynthesized Ag-NPs exhibited significant antibacterial activity against different clinically important pathogenic microorganisms (*E. coli* and *S. aureus*) and they also exhibited a good inhibitory effect on *E. coli* biofilms.
4. The synthesized Ag-NPs displayed significant antioxidant, antibacterial, and antibiofilm activities, demonstrating their potential in biomedical and industrial applications. Additionally, the photocatalytic degradation of methylene blue (MB) by these nanoparticles highlights their efficiency in environmental remediation.
5. Consequently, it can be said that the use of Ag-NPs synthesized via green synthesis is promising in various fields.

Conflicts of Interest

The author declares no conflict of interest.

REFERENCES CITED

Abid, J. P., Wark, A. W., Brevet, P. F., and Girault, H. H. (2002). "Preparation of silver nanoparticles in solution from a silver salt by laser irradiation," *Chem. Commun.*7, 792-793. DOI: 10.1039/b200272h

Abishad, P., Vergis, J., Unni, V., Ram, V. P., Niveditha, P., Yasur, J., Juliet, S., John, L., Byrappa, K., Nambiar, P., *et al*. (2022). "Green synthesized silver nanoparticles using

Lactobacillus acidophilus as an antioxidant, antimicrobial, and antibiofilm agent against multi-drug resistant enteroaggregative *Escherichia coli*," *Probiotics Antimicrob. Proteins* 14(5), 904-914. DOI: 10.1007/s12602-022-09961-1

Ahmed, S., Ahmad, M., Swami, B. L., and Ikram, S. (2016). "Green synthesis of silver nanoparticles using *Azadirachta indica* aqueous leaf extract," *J. Radiat. Res. Appl. Sci.* 9(1), 1-7. DOI: 10.1016/j.jrras.2015.06.006

Akkol, E. K., Yeşilada, E., and Güvenç, A. (2008). "Valuation of anti-inflammatory and antinociceptive activities of *Erica* species native to Turkey," *J. Ethnopharmacol.* 116(2), 251-257. DOI: 10.1016/j.jep.2007.11.023

Alarcon, E. I., Udekwu, K., Skog, M., Pacioni, N. L., Stamplecoskie, K. G., González-Béjar, M., Polisetti, N., Wickham, A., Richter-Dahlfors, A., Griffith, M., *et al.* (2012). "The biocompatibility and antibacterial properties of collagen-stabilized, photochemically prepared silver nanoparticles," *Biomaterials* 33(19), 4947-4956. DOI: 10.1016/j.biomaterials.2012.03.033

Anandalakshmi, K., Venugobal, J., and Ramasamy, V. (2016). "Characterization of silver nanoparticles by green synthesis method using *Pedalium murex* leaf extract and their antibacterial activity," *Appl. Nanosci.* 6, 399-408. DOI: 10.1007/s13204-015-0449-z

Ansari, M. A., Kalam, A., Al-Sehemi, A. G., Alomary, M. N., AlYahya, S., Aziz, M. K., Srivastava, S., Alghamdi, S., Akhtar, S., Almalki, H. D., *et al*. (2021). "Counteraction of biofilm formation and antimicrobial potential of *Terminalia catappa* functionalized silver nanoparticles against *Candida albicans* and multidrug-resistant Gram-negative and Gram-positive bacteria," *Antibiotics* 10(6), article 725. DOI: 10.3390/antibiotics10060725

Arshad, M., Khan, A., Farooqi, Z. H., Usman, M., Waseem, M. A., Shah, S. A., and Khan, M. (2018). "Green synthesis, characterization and biological activities of silver nanoparticles using the bark extract of *Ailanthus altissima*," *Mater. Sci. Pol.* 36(1), 21-26. DOI: 10.1515/msp-2017-0100

Asiabar, F. G, Mirzaie, A., and Arasteh, J. (2019). "Antibacterial and cytotoxicity of synthesized silver nanoparticles using *Erica carnea* extract on breast cancer cell line (MCF-7) and analysis of its apoptotic effects," *Razi J. Med Sci.* 26(6), 84-94. DOI: 10.5555/20203323582

Bar, H., Bhui, D. K., Sahoo, G. P., Sarkar, P., Pyne, S., and Misra, A. (2009). "Green synthesis of silver nanoparticles using seed extract of *Jatropha curcas*," *Colloids Surf. A: Physicochem. Eng.* 348(1-3), 212-216. DOI: 10.1016/j.colsurfa.2009.07.021

Begum, I., Shamim, S., Ameen, F., Hussain, Z., Bhat, S. A., Qadri, T., and Hussain, M. (2022). "A combinatorial approach towards antibacterial and antioxidant activity using tartaric acid capped silver nanoparticles," *Processes* 10(4), article 716. DOI: 10.3390/pr10040716

Bommakanti, V., Banerjee, M., Shah, D., Manisha, K., Sri, K., and Banerjee, S. (2022). "An overview of synthesis, characterization, applications and associated adverse effects of bioactive nanoparticles," *Environ. Res.* 214, 113919, 1-15. DOI: 10.1016/j.envres.2022.113919

Chen, P., Song, L., Liu, Y., and Fang, Y. (2007). "Synthesis of silver nanoparticles by gamma-ray irradiation in acetic water solution containing chitosan," *Radiat. Phys. Chem.* 76, 1165-1168. DOI: 10.1016/j.radphyschem.2006.11.012

Clogston, J. D., and Patri, A. K. (2011). "Zeta potential measurement," *Characterization of nanoparticles intended for drug delivery, Methods in Molecular Biology,* 63-70. DOI: 10.1007/978-1-60327-198-1_6

Domínguez, A. V., Algaba, R. A., Canturri, A. M., Villodres, Á. R., and Smani, Y. (2020). "Antibacterial activity of colloidal silver against gram-negative and gram-positive bacteria," *Antibiotics (Basel)*, 9(1), article 36. DOI: 10.3390/antibiotics9010036

Dwivedi, A. D., and Gopal, K. (2010). "Biosynthesis of silver and gold nanoparticles using *Chenopodium album* leaf extract," *Colloids Surf. A: Physicochem. Eng.* 369, 27-33. DOI: 10.1016/j.colsurfa.2010.07.020

Du, J., Singh, H., and Yi, T. H. (2016). "Antibacterial, anti-biofilm and anticancer potentials of green synthesized silver nanoparticles using benzoin gum (*Styrax benzoin*) extract," *Bioprocess. Biosyst. Eng.* 39, 1923-1931. DOI: 10.1007/s00449-016-1666-x

Dubey, S. P., Lahtinen, M., and Sillanpaa, M. (2010). "Green synthesis and characterization of silver and gold nanoparticles using leaf extract of *Rosa rugosa*," *Colloids Surf. A: Physicochem. Eng.* 364, 34-41. DOI: 10.1016/j.colsurfa.2010.04.023

Elumalai, D., Hemavathi, M., Deepaa, C. V., and Kaleena, P. K. (2017). "Evaluation of photosynthesized silver nanoparticles from leaf extracts of *Leucas aspera* and *Hyptis suaveolens* and their larvicidal activity against malaria, dengue and filariasis vectors," *Parasite Epidemiol. Control.* 2(4), 15-26. DOI: 10.1016/j.parepi.2017.09.001

Erci, F., Cakir-Koc, R., and Isildak, I. (2018). "Green synthesis of silver nanoparticles using *Thymbra spicata* L. var. *spicata* (zahter) aqueous leaf extract and evaluation of their morphology-dependent antibacterial and cytotoxic activity," *Artif. Cells Nanomed. Biotechnol.* 46(Sup1), 150-158. DOI: 10.1080/21691401.2017.1415917

Erci, F., and Torlak, E. (2019). "Antimicrobial and antibiofilm activity of green synthesized silver nanoparticles by using aqueous leaf extract of *Thymus serpyllum*," *Sakarya Uni. J. Sci.* 23(3), 333-339. DOI: 10.16984/saufenbilder.445146

Fafal, T. Taştan, P., Tüzün, B. S., Ozyazici, M., and Kivcak, B. (2017). "Synthesis, characterization and studies on antioxidant activity of silver nanoparticles using *Asphodelus aestivus* Brot. aerial part extract," *S. Afr. J. Bot.* 112, 346-353. DOI: 10.1016/j.sajb.2017.06.019

Flores-Ramírez, A. Y., Aguilera-Aguirre, S., Chacón-López, M. A., Ortiz-Frade, L. A., Antaño-López, R., Álvarez-López, A., Rodríguez-López, A., and López-García, U. M. (2023). "Physicochemical–electrochemical characterization of the nanocomposite chitosan-coated magnetite nanoparticles," *J. Clust. Sci.* 34(2), 1019-1035. DOI: 10.1007/s10876-022-02278-7

Geethalakshmi, R., and Sarada, D. V. L. (2010). "Synthesis of plant-mediated silver nanoparticles using *Trianthema decandra* extract and evaluation of their anti-microbial activities," *Int. J. Eng. Sci.* 2, 970-975.

Goudarzi, M., Mir, N., Mousavi-Kamazani, M., Bagheri, S., and Salavati-Niasari, M. (2016). "Biosynthesis and characterization of silver nanoparticles prepared from two novel natural precursors by facile thermal decomposition methods," *Sci. Rep.* 6(1), article ID 32539. DOI: 10.1038/srep32539

Gudikandula, K., and Charya Maringanti, S. (2016). "Synthesis of silver nanoparticles by chemical and biological methods and their antimicrobial properties," *J. Exp. Nanosci.* 11(9), 714-721. DOI: 10.1080/17458080.2016.1139196

Gupta, K., Hazarika, S. N., Saikia, D., Namsa, N. D., and Mandal, M. (2014). "One step green synthesis and anti-microbial and anti-biofilm properties of *Psidium guajava* L. leaf extract-mediated silver nanoparticles," *Mater. Lett.* 125, 67-70. DOI: 10.1016/j.matlet.2014.03.134

Guzman, M., Dille, J., and Godet, S. (2012). "Synthesis and antibacterial activity of silver nanoparticles against gram-positive and gram-negative bacteria," *Nanomed: Nanotechnol. Bio. Med.* 8(1), 37-45. DOI: 10.1016/j.nano.2011.05.007

Jacob, S. J. P., Finub, J. S., and Narayanan, A. (2012). "Synthesis of silver nanoparticles using *Piper longum* leaf extracts and its cytotoxic activity against Hep-2 cell line," *Colloids Surf.* 91, 212-214. DOI: 10.1016/j.colsurfb.2011.11.001

Jha, A. K., and Prasad, K. (2010). "Green synthesis of silver nanoparticles using *Cycas* leaf," *Int. J. Green Nanotechnol.* 1, 110-1117. DOI: 10.1080/19430871003684572

Jyoti, K., Baunthiyal, M., and Singh, A. (2016). "Characterization of silver nanoparticles synthesized using *Urtica dioica* Linn. leaves and their synergistic effects with antibiotics," *J. Radiat. Res. Appl. Sci.* 9(3), 217-227. DOI: 10.1016/j.colsurfa.2020.124827

Kalaycıoğlu, Z., Özuğur Uysal, B., Pekcan, Ö., and Erim, F. B. (2023). "Efficient photocatalytic degradation of methylene blue dye from aqueous solution with cerium oxide nanoparticles and graphene oxide-doped polyacrylamide," *ACS Omega* 8, 13004-13015. DOI: 10.1021/acsomega.3c00198

Kanniah, P., Chelliah, P., Thangapandi, J. R., Gnanadhas, G., Mahendran, V., and Robert, M. (2021). "Green synthesis of antibacterial and cytotoxic silver nanoparticles by *Piper nigrum* seed extract and development of antibacterial silver-based chitosan nanocomposite," *Int. J. Biol. Macromol.* 189, 18-33. DOI: 10.1016/j.ijbiomac.2021.08.056

Khan, A., El-Toni, A. M., Alrokayan, S., Alsalhi, M., Alhoshan, M., and Aldwayyan, A. S. (2011). "Microwave-assisted synthesis of silver nanoparticles using poly-N isopropyl acrylamide/acrylic acid microgel particles," *Colloids Surf. A: Physicochem. Eng.* 377, 356-360. DOI: 10.1016/j.colsurfa.2011.01.042

Khan, A. U., Yuan, Q., Wei, Y., Khan, Z. H., Tahir, K., Khan, S. U., Ahmad, A., Khan, S., Nazir, S., and Khan, F. U. (2016). "Ultra-efficient photocatalytic deprivation of methylene blue and biological activities of biogenic silver nanoparticles," *J. Photochem. Photobiol. B- Biol.* 159, 49-58. DOI: 10.1016/j.jphotobiol.2016.03.017

Khalil, M. M. H., Ismail, E. H., El-Baghdady, K. Z., and Mohamed, D. (2014). "Green synthesis of silver nanoparticles using olive leaf extract and its antibacterial activity," *Arab. J. Chem.* 7(6), 1131-1139. DOI: 10.1016/j.arabjc.2013.04.007

Kıvçak, B., Fafal Erdoğan, T., Gönenç, T., Pabuçcuoglu, A., Oran, E., Kahraman, F., and Öztürk, T. (2013). "Antioxidant, antimicrobial and cytotoxic activities of *Erica bocquetii PF Stevens* and *Erica arborea* L.," *Gumushane Uni. J. Health. Sci.* 2(1), 52-65.

Koroglu, A., Hurkul, M. M., Kendir, G., and Kucukboyaci, N. (2019). "*In vitro* antioxidant capacities and phenolic contents of four *Erica* L. (Ericaceae) taxa native to Turkey," *J. Res. Pharm.* 23(1), 93-100. DOI: 10.12991/jrp.2018.113

Krishnaraj, C., Jagan, E. G., Rajasekar, S., Selvakumar, P., Kalaichelvan, P. T., and Mohan, N. (2010). "Synthesis of silver nanoparticles using *Acalypha indica* leaf extracts and its antibacterial activity against water borne pathogens," *Colloids Surf. B.* 70, 50-56. DOI: 10.1016/j.colsurfb.2009.10.008

Kwon, G. J., Han, S. Y., Park, C. W., Park, J.S., Lee, E. A., Kim, N. H., Alle, M., Bandi, R., and Lee, S. H. (2020). "Adsorption characteristics of Ag nanoparticles on cellulose nanofibrils with different chemical compositions," *Polymers* 12(1), article 164. DOI: 10.3390/polym12010164

Li, R., Pan, Y., Li, N., Wang, Q., Chen, Y., Phisalaphong, M., and Chen, H. (2020). "Antibacterial and cytotoxic activities of a green synthesized silver nanoparticles using corn silk aqueous extract," *Colloids Surf. A: Physicochem. Eng.* 598, article ID 124827. DOI: 10.1016/j.colsurfa.2020.124827

Li, S., Shen, Y., Xie, A., Yu, X., Qiu, L., Zhang, L., and Zhang, Q. (2007). "Green synthesis of silver nanoparticles using *Capsicum annuum L.* extract," *Green Chem.* 9(8), 852-858. DOI: 10.1039/B615357G

Mallick, K., Witcomb, M. J., and Scurrell, M. S. (2004). "Polymer stabilized silver nanoparticles: A photochemical synthesis route," *J. Mater. Sci.* 39, 4459-4463. DOI: 10.1023/B:JMSC.0000034138.80116.50

Marslin, G., Siram, K., Maqbool, Q., Selvakesavan, R. K., Kruszka, D., Kachlicki, P., and Franklin, G. (2018). "Secondary metabolites in the green synthesis of metallic nanoparticles," *Materials*, 11(6), 940, 1-25. DOI: 10.3390/ma11060940

Miri, A., Shahraki Vahed, H. O., and Sarani, M. (2018). "Biosynthesis of silver nanoparticles and their role in photocatalytic degradation of methylene blue dye," *Rev. Chem. Intermed.* 44, 6907-6915. DOI: 10.1007/s11164-018-3529-3

Moosa, A. A., Ridha, A. M. and Allawi, M. H. (2015). "Green synthesis of silver nanoparticles using spent tea leaves extract with atomic force microscopy," *Int. J. Recent. Technol. Eng.* 5(5), 3233-3241.

Mukherjee, S., Chowdhury, D., Kotcherlakota, R., Patra, S., Vinothkumar, B., Bhadra, M. P., Sreedhar, B., and Patra, C. R. (2014). "Potential theranostics application of bio-synthesized silver nanoparticles (4-in-1 system)," *Theranostics* 4, 316-335. DOI: 10.7150/thno.7819

Mukunthan, K. S., Elumalai, E. K., Patel, T. N., and Murty, V. R. (2011). "*Catharanthus roseus*: A natural source for the synthesis of silver nanoparticles," *Asian Pac. J. Trop. Biomed.* 1, 270-274. DOI: 10.1016/S2221-1691(11)60041-5

Naidjonoka, P., Fornasier, M., Pålsson, D., Rudolph, G., Al-Rudainy, B., Murgia, S., and Nylander, T. (2021). "Bicontinuous cubic liquid crystalline phase nanoparticles stabilized by softwood hemicellulose," *Colloids Surf. B: Biointer.* 203, article 111753. DOI: 10.1016/j.colsurfb.2021.111753

Panáček, A., Prucek, R., Hrbac, J., Nevečná, T. J., Steffkova, J., Zboril, R., and Kvitek, L. (2014). "Polyacrylate-assisted size control of silver nanoparticles and their catalytic activity," *Chem. Mater.* 26, 1332-1339. DOI: 10.1021/cm400635z

Ravichandran, V., Vasanthi, S., Shalini, S., Shah, S. A. A., and Harish, R. (2016). "Green synthesis of silver nanoparticles using *Atrocarpus altilis* leaf extract and the study of their antimicrobial and antioxidant activity," *Mater. Lett.* 180, 264-267. DOI: 10.1016/j.matlet.2016.05.172

Patil, S. V., Borase, H. P., Patil, C. D., and Salunke, B. K. (2012). "Biosynthesis of silver nanoparticles using latex from few *Euphorbian* plants and their antimicrobial potential," *Appl. Biochem. Biotechnol.* 167, 776-790. DOI: 10.1007/s12010-012-9710-z

Patil, M. P., Singh, R. D., Koli, P. B., Patil, K. T., Jagdale, B. S., Tipare, A. R., and Kim, G. D. (2018). "Antibacterial potential of silver nanoparticles synthesized using *Madhuca longifolia* flower extract as a green resource," *Microb. Pathog.* 121, 184-189. DOI: 10.1016/j.micpath.2018.05.040

Pavlović, R. D., Lakušićć, B., Došlov-Kokoruš, Z., and Kovačević, N. (2009). "Arbutin content and antioxidant activity of some Ericaceae species," *Pharmazie* 64(10), 656-659. DOI: 10.1691/ph.2009.9551

Prakash, P., Gnanaprakasam, P., Emmanuel, R., Arokiyaraj, S., and Saravanan, M. (2013). "Green synthesis of silver nanoparticles from leaf extract of *Mimusops elengi, Linn.* for enhanced antibacterial activity against multi drug resistant clinical isolates," *Colloids Surf. B: Biointer.* 108, 255-259. DOI: 10.1016/j.colsurfb.2013.03.017

Prasad, K. S., Pathak, D., Patel, A., Dalwadi, P., Prasad, R., Patel, P., and Selvaraj, K. (2011). "Biogenic synthesis of silver nanoparticles using *Nicotiana tobaccum* leaf extract and study of their antibacterial effect," *Afr. J. Biotechnol.* 10, 8122-8130. DOI: 10.5897/AJB11.394

Rao, Y. S., Kotakadi, V. S., Prasad, T. N. V. K. V., Reddy, A. V., and Sai Gopal, D. V. R. (2013). "Green synthesis and spectral characterization of silver nanoparticles from Lakshmi tulasi (*Ocimum sanctum*) leaf extract," *Spectrochim. Acta A Mol.Biomol. Spectrosc.* 103, 156-159. DOI: 10.1016/j.saa.2012.11.028

Reicha, F. M., Sarhan, A., Abdel-Hamid, M. I., and El-Sherbiny, I. M. (2012). "Preparation of silver nanoparticles in the presence of chitosan by electrochemical method," *Carbohydr. Polym.* 89, 236-244. DOI: 10.1016/j.carbpol.2012.03.002

Reyes Ruiz, M., Martin-Cordero, C., Ayuso Gonzalez, M. J., Toro Sainz, M. V., and Alarcon de la Lastra C. (1996). "Antiulcer activity in rats by flavonoids *of Erica andevalensis* Cabezudo-Rivera," *Phytother. Res.* 10(4), 300-303. DOI: 10.1002/(SICI)1099-1573(199606)10:4<300::AID-PTR844>3.0.CO;2-Z

Saxena, A., Tripathi, R.M., Zafar, F., and Singh P. (2012). "Green synthesis of silver nanoparticles using aqueous solution of *Ficus benghalensis* leaf extract and characterization of their antibacterial activity," *Mater. Lett.* 67, 91-94. DOI: 10.1016/j.matlet.2011.09.038

Singh, P., Pandit, S., Mokkapati, V. R. S. S., Garnæs, J., and Mijakovic, I. (2020). "A sustainable approach for the green synthesis of silver nanoparticles from *Solibacillus isronensis sp.* and their application in biofilm inhibition," *Molecules,* 25(12), 2783, 1-16. DOI: 10.3390/molecules25122783

Singla, S., Jana, A., Thakur, R., Kumari, C., Goyal, S., and Pradhan, J. (2022). "Green synthesis of silver nanoparticles using *Oxalis griffithii* extract and assessing their antimicrobial activity," *OpenNano* 7, article ID 100047. DOI: 10.1016/j.onano.2022.100047

Somasundaram, C. K., Atchudan, R., Edison, T. N. J. I., Perumal, S., Vinodh, R., Sundramoorthy, A. K., Babu, R. S., Alagan, M., and Lee, Y. R. (2021). "Sustainable synthesis of silver nanoparticles using marine algae for catalytic degradation of methylene blue," *Catalysts* 11(11), article 1377. DOI: 10.3390/catal11111377

Sreelekha, E., George, B., Shyam, A., Sajina, N., and Mathew, B. (2021). "A comparative study on the synthesis, characterization, and antioxidant activity of green and chemically synthesized silver nanoparticles," *BioNanoScience* 11, 489-496. DOI: 10.1007/s12668-021-00824-7

Srikar, S. K., Giri, D. D., Pal, D. B., Mishra, P. K., and Upadhyay, S. N. (2016). "Green synthesis of silver nanoparticles: A review," *Green and Sustain. Chem.* 6(1), 34-56. DOI: 10.4236/gsc.2016.61004

Sun, Q., Cai, X., Li, J., Zheng, M., Chen, Z., and Yu, C. P. (2014). "Green synthesis of silver nanoparticles using tea leaf extract and evaluation of their stability and antibacterial activity," *Colloids Surf. A: Physicochem. Eng.* 444, 226-231. DOI: 10.1016/j.colsurfa.2013.12.065

Veerasamy, R., Xin T. Z., Gunasagaran S., Xiang T. F. W., Yang E. F. C., Jeyakumar N., and Dhanaraj S. A. (2011). "Biosynthesis of silver nanoparticles using mangosteen

leaf extract and evaluation of their antibacterial activities," *J. Saudi Chem. Soc.* 15, 113-120. DOI: 10.1016/j.jscs.2010.06.004

Vidhu, V. K., Aromal, S. A., and Philip D. (2011). "Green synthesis of silver nanoparticles using *Macrotyloma uniflorum*," *Spectrochimica Acta - A: Mol. Biomol. Spectrosc.* 83, 392-397. DOI: 10.1016/j.saa.2011.08.051

Ulug, B., Turkdemir, M. H., Cicek, A., and Mete, A. (2015). "Role of irradiation in the green synthesis of silver nanoparticles mediated by fig *(Ficus carica)* leaf extract," *Spectrochim Acta A Mol Biomol Spectrosc.* 135, 153-161. DOI: 10.1016/j.saa.2014.06.142

Wang, L., Wu, Y., Xie, J., Wu, S., and Wu, Z. (2018). "Characterization, antioxidant and antimicrobial activities of green synthesized silver nanoparticles from *Psidium guajava L.* leaf aqueous extracts," *Mater. Sci. Eng. C* 86, 1-8.

Wei, S., Wang, Y., Tang, Z., Xu, H., Wang, Z., Yang, T., and Zou, T. (2021). "A novel green synthesis of silver nanoparticles by the residues of Chinese herbal medicine and their biological activities," *RSC Adv.* 11(3), 1411-1419. DOI: 10.1039/D0RA08287B

Yang, J., and Pan, J. (2012). "Hydrothermal synthesis of silver nanoparticles by sodium alginate and their applications in surface-enhanced Raman scattering and catalysis," *Acta Mater.* 60, 4753-4758. DOI: 10.1016/j.actamat.2012.05.037

Yang, F., Zhang, Z., and Yang, C. Y. (2017). "A laboratory demonstration for the estimation of the percentage of oxygen in air," *J. Lab. Chem. Educ.* 5(5), 116-119. DOI: 10.5923/j.jlce.20170505.03

Yilmaz, M., Turkdemir, H., Kilic, M. A., Bayram, E., Cicek, A., Mete, A., and Ulug, B. (2011). "Biosynthesis of silver nanoparticles using leaves of *Stevia rebaudiana*," *Mater. Chem. Phys.* 130, 1195-1202. DOI: matchemphys.2011.08.068

Zaheer, Z. (2012). "Silver nanoparticles to self-assembled films: green synthesis and characterization," *Colloids Surf. B- Biointer.* 90, 48-52. DOI: 10.1016/j.colsurfb.2011.09.037

Zhang, X. F., Liu, Z. G., Shen, W., and Gurunathan, S. (2016). "Silver nanoparticles: synthesis, characterization, properties, applications, and therapeutic approaches," *Int. J. Mol. Sci.* 17(9), article 1534. DOI: 10.3390/ijms17091534

Zheng, Y., Cao, L., Xing, G., Bai, Z., Huang, J. and Zhang, Z. (2019). "Microscale flower-like magnesium oxide for highly efficient photocatalytic degradation of organic dyes in aqueous solution," *RSC Adv.*, 9(13), 7338-7348. DOI: 10.1039/C8RA10385B

Article submitted: February 26, 2024; Peer review completed: March 16, 2024; Revised version received: March 24, 2024; Accepted: March 26, 2024; Published: May 16, 2024.
DOI: 10.15376/biores.19.3.4396-4422